J. Condensed Matter Nucl. Sci. 13 (2014) 89–105

Research Article

Changes Observed in the Elemental Composition of Palladium and Rhenium Specimens Irradiated in Dense Deuterium by γ-Quanta with Boundary of Energy 23 MeV

A.Yu. Didyk*

Joint Institute for Nuclear Research, 141980 Dubna, Russia

R. Wisniewski†

National Center of Nuclear Research, 05-400 Otwock, Poland

Abstract

We have studied the elemental composition of palladium and rhenium specimens irradiated in dense gaseous deuterium by γ-quanta of a continuous spectrum with the threshold energy of 23 MeV. Significant anomalies are found in the structure and elemental composition of the irradiated specimens. At both ends of the palladium wire considerable changes are observed in the form of blowouts (resembling congealed "Solar protuberances") of molten metal with complex elemental composition. The palladium surface proved to be covered with small particles, approximately 1–2 μm in size, composed of rhenium oxide Re_2O_7 , while near the cracks and fractures the surface was covered with rhenium, carbon and oxygen crystallites of hexagonal symmetry. The entire surface of the rhenium sample became cracked and coated with a thick layer of carbon compounds with rhenium as Re_xC_y. The phenomenological model of nuclear reactions leading to the observed elemental composition of rhenium and palladium is discussed.
 ISSN 2227-3123

Keywords: Chain reaction of deuterium heating, Dense deuterium gas, Elastic and inelastic scattering, ^{2}H-induced reactions, High pressure, Photon absorption and scattering

1. Introduction

In previous works [1–6] the authors described a new approach to the study of nuclear reactions in deuterated materials saturated with atomic deuterium up to stoichiometric composition [7,8]. The authors described the creation of new structures in dense gaseous deuterium in metals. This approach is based on: (a) the use of Deuterium High Pressure Chambers (DHPC), see [6], which are capable of preserving molecular deuterium in a gaseous state for a long time

*E-mail: didyk@jinr.ru
†E-mail: roland.wisniewski@gmail.com

 ISSN 2227-3123

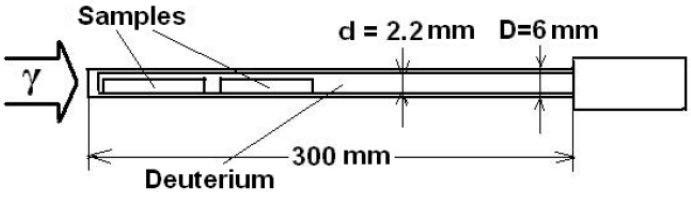

Figure 1. A schematic of the Deuterium High Pressure Chamber (DHPC) used to irradiate materials.

under pressure of up to 3–4 kbar, (b) application in HPC filled with dense gaseous molecular deuterium in which metallic or non-metallic specimens and special collectors for synthesized structures are placed, (c) irradiation of the DHPC by a flux of γ-quanta with a continuous energy spectrum, obtained at the tungsten braking target using electron beams of energies 10–25 MeV, i.e., in the region of a giant dipole resonance.

The aim of this work is to study the characteristics of nuclear reaction processes in pure metals in these conditions.

2. Experimental Technique

Palladium specimens (99.96%, in the shape of a wire of diameter 1 mm and length 110.7 mm) and rhenium specimens (99.97%, three wires of diameter 1 mm and lengths 12.5, 24.5 and 33.0 mm) were placed in a DHPC under the pressure of gaseous deuterium 2860 bar and irradiated at the electron accelerator MT-25 by electrons of energy 23.5 MeV at the average electron beam current 11–12 μA during 17.5 h of pure accelerator time.

Figure 1 shows a DHPC used for γ-quanta irradiation of specimens of various materials in the shape of wires and cylinders with relatively small diameters.

It should be noted that in the first experiment, which was described in detail in [1–5], a patented DHPC chamber [6] was used. In this experiment the walls of the DHPC constructed in frames of another project are made of 206 stainless steel to exclude chemical elements such as copper and zinc, which were observed in the first experiment. These elements formed contamination that made up a layer 80 μm thick on the palladium in the first experiment.

In the present experiment the thickness (W) of the braking target was set to 3 mm, while the aluminum electron absorber was 25 mm. Irradiation by γ-quanta with threshold energy 23 MeV was carried out for 19.5 h (7×10^4 s) at the average electron beam current 11–12 μmÀ. Calculation of γ-quanta spectra and fluxes as well as neutron yield from the d(γ,n)p neutron photodisintegration reaction is described in detail in [1–5].

Before opening the DHPC (Fig. 1), the chamber pressure was measured to be 2860 bar. The palladium (99.96%, a wire of length 110 mm and diameter 1 mm) and rhenium (99.97%, three wires of lengths 12, 25 and 33 mm and diameter 1 mm) specimens placed in the chamber could be extracted only three days after deuterium desorption. The specimens, like the DHPC itself, proved to be highly activated, which prevented X-ray microelement analysis even after a long period of waiting for decreased induced activity: four full months for the palladium specimens and over eight months for the rhenium ones. As in previous studies [2–4], investigation of the structure and elemental composition of the virgin and irradiated specimens was done using scanning electron microscopy (SEM) and X-ray microelement analysis (XMA).

2.1. Experimental results for the palladium wire of length 110.7 mm

As shown in Fig. 2, the right edge of the specimen has undergone particularly considerable changes, namely, formation of an elongated part tapering towards the end from 1 to 0.461 mm in diameter with a strongly deformed frontal edge

Table 1. Shows element concentrations at Points 1–3.

Element	Z	X-rayseries	Point 1		Point 2		Point 3	
			wt.%	at.%	wt.%	at.%	wt.%	at.%
C	6	K	–	–	65.24	76.22	48.31	66.42
O	8	K	15.24	27.95	18.04	15.77	14.30	14.76
F	9	K	–	–	–	–	7.52	6.28
Na	11	K	–	–	0.88	0.53	1.61	1.16
Mg	12	K	2.22	2.68	0.45	0.26	–	–
Al	13	K	50.18	54.56	12.06	6.26	12.99	7.95
Si	14	K	3.14	3.28	0.14	0.07	–	–
S	16	K	1.04	0.95	0.11	0.05	–	–
Cl	17	K	0.50	0.41	0.48	0.19	0.24	0.11
K	19	K	1.89	1.42	0.44	0.16	3.45	1.46
Ca	20	K	0.71	0.52	0.09	0.03	0.58	0.24
Cr	24	K	0.96	0.54	0.30	0.08	0.47	0.15
Mn	25	K	0.63	0.33	0.06	0.02	–	–
Fe	26	K	4.51	2.37	1.37	0.34	2.52	0.75
Ni	28	K	–	–	0.10	0.02	–	–
Cu	29	K	4.05	1.87	0.05	0.01	–	–
Zn	30	K	2.29	1.03	–	–	–	–
Pd	46	L	0.83	0.23	–	–	–	–
Re	75	L	11.82	1.86	–	–	8.32	0.74

about 100 μm wide. On both at the left (a) and right (b) ends of the wire one can observe smaller-scale inhomogeneities in the shape of congealed blowouts from the surfaces.

Figure 3 shows congealed-"Solar-protuberances" structures: (a) – blowout from the left surface in the direction opposite to the γ-quanta flux direction, (b) – blowout in the direction coinciding with the γ-quanta flux direction, and (c) – "pedestal" crystal structure on the surface from the direction of γ-quanta penetration.

Table 1 clearly shows that nuclear reactions in this experiment produce such palladium fission products as copper ($_{29}$Cu–1.87 at.%) and zinc ($_{30}$Zn–1.03 at.%). These results are similar to the results presented in [1–5]. One can also see that nuclear reactions in palladium yield light chemical elements $_{12}$Mg, $_{13}$Al, $_{14}$Si. $_{16}$S, $_{17}$Cl, $_{19}$K and $_{20}$Ca, heavier elements $_{24}$Cr, $_{25}$Mn, $_{26}$Fe, also $_{29}$Cu and $_{30}$Zn. The latter two chemical elements deserve special attention because they were found in significant quantities in the palladium cylinder surface in studies [1–5]. In order to check the reaction

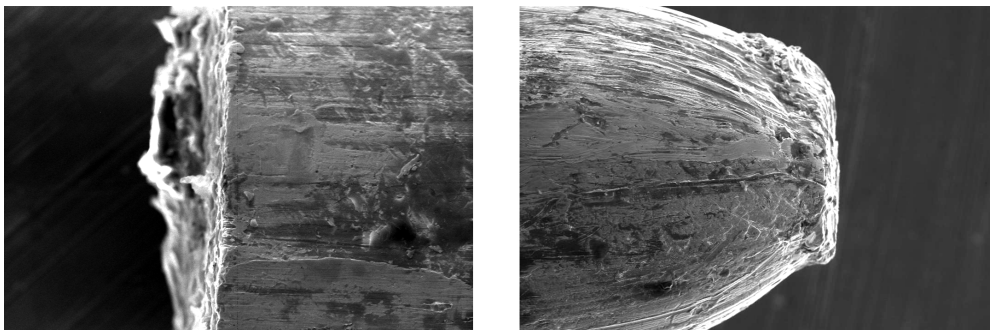

Figure 2. SEM images of the left (a) and right ends of the palladium wire.

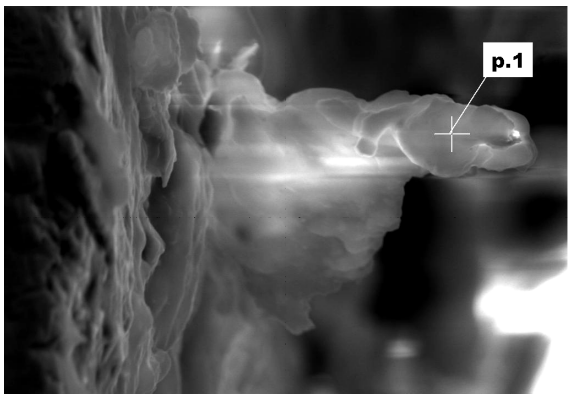

(a)

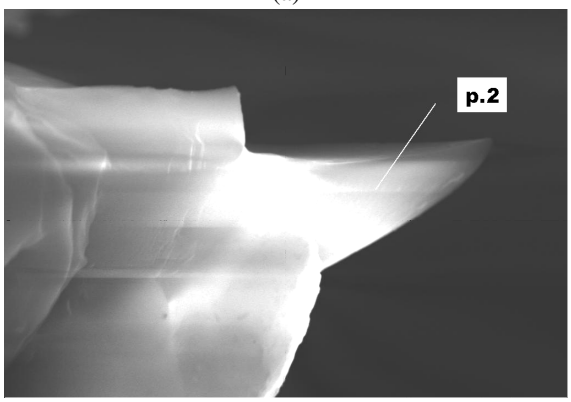

(b)

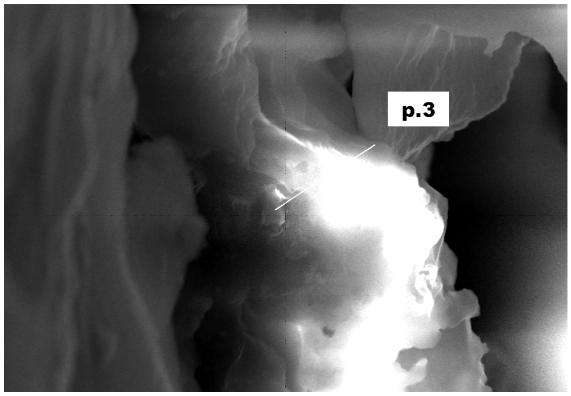

(c)

Figure 3. Two congealed blowouts from the direction of γ-quanta entry into the left end of the palladium wire and the "pedestal" of structure (Fig. 4).

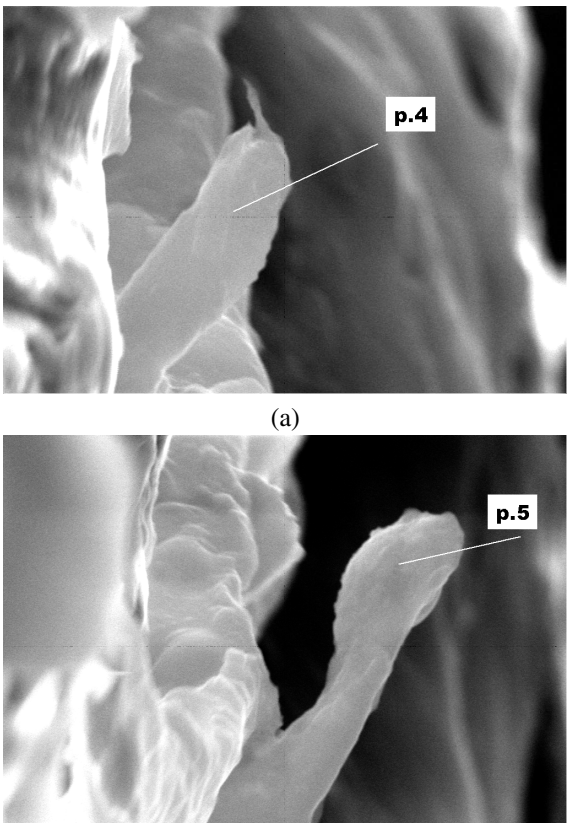

(a)

(b)

Figure 4. Two congealed blowouts from the direction of γ-quanta escape from the right end of the palladium wire.

processes in palladium with the production of $_{29}$Cu and $_{30}$Zn, all the materials containing these elements in the previous DHPC were replaced with stainless steel (see Fig. 1).

Figure 4 shows two photos of blowouts at the end surface, from the direction coinciding with the γ-quanta flux direction. As is shown, the elemental composition of the blowouts is comprised of a series of elements, which are lighter than palladium. Moreover, these elements are by no means coincidental. They can be obtained in nuclear reactions via fission of palladium isotopes which are described in [3,5]. The atoms of light chemical elements as $_{11}$Na, $_{12}$Mg, $_{13}$Al, $_{14}$Si, $_{16}$S, $_{17}$Cl, $_{19}$K, $_{20}$Ca, $_{24}$Cr, $_{25}$Mn, $_{26}$Fe, and $_{28}$Ni have greater volatility than the atoms of heavy chemical elements such as $_{46}$Pd; therefore, the palladium concentration is small or completely absent from the chemical composition of the congealed blowout (see Table 2). The speed of particle evaporation from the surface, introduced in [9], represents as

$$\frac{\mathrm{d}n}{\mathrm{d}t} = N\left(\frac{kT}{2\pi M}\right)^{1/2} \exp\left[-\frac{U_0}{kT}\right],$$

where N, k, T, M, and U_0 are the atomic density of particles in liquid phase, Boltzmann's constant, temperature on the surface, mass of the escaping particle and particle-surface binding energy, respectively.

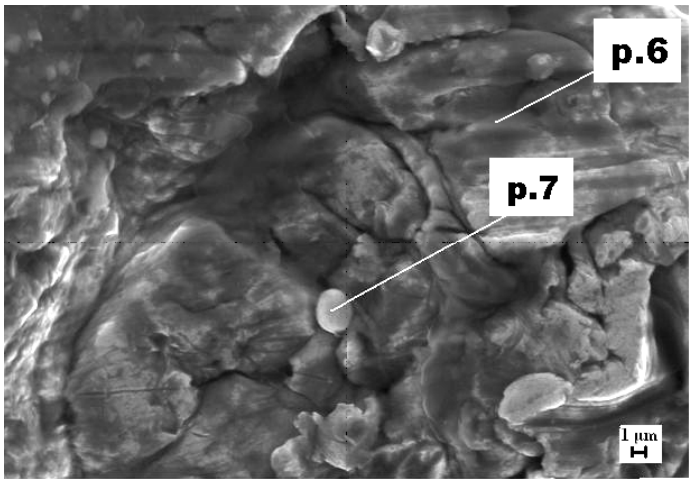

Figure 5. SEM image of surface patch near the tapering part from Fig. 2 (b).

Table 2 shows congealed blowouts of the elemental compositions in the cavities at Points 4 and 5. In Fig. 4, the SEM image shows a surface patch near the tapering part (Fig. 2 (b)) with two points where XMA analysis was carried out.

As is evident from Table 3 (Point 6), when the palladium concentration is significantly high, iron, nickel and chromium are also present. The composition of these elements is close to the elemental composition of the 206 stainless steel, which comprises the material of the DHPC wall: Fe-60.4%; Cr-30.5%, and Ni-9.0%. Nevertheless, the measured concentration of these elements is different from the original construction stainless steel composition. Apart from this, one can also observe significant amounts of aluminum (17.29 at.%) and copper (2.02 at.%). Analysis of a particle observed on the palladium wire surface (at Point 7) revealed a high concentration, for instance, of iron (38.39 at.%) and also carbon (37.76 at.%).

Table 2. Shows the elemental compositions in the cavities at Points 4 and 5.

Element	Z	X-ray series	Point 4		Point 5	
			wt.%	at.%	wt.%	at.%
$_6$C	6	K	30.40	47.58	–	–
$_8$O	8	K	9.52	11.42	10.82	18.19
Na	11	K	–	–	1.36	1.59
Mg	12	K	1.32	1.02	1.67	1.85
Al	13	K	55.14	38.42	68.73	58.55
Si	14	K	0.37	0.45	1.58	1.51
S	16	K	0.11	0.07	0.29	0.25
Cl	17	K	0.74	0.39	0.77	0.58
K	19	K	0.43	0.20	0.64	0.44
Ca	20	K	0.27	0.13	5.74	3.86
Cr	25	K	0.29	0.10	0.83	0.43
Mn	25	K	0.36	0.12	0.58	028
Fe	26	K	0.82	0.28	2.20	1.06
Ni	28	K	0.02	0.01	0.95	0.44
Pd	46	L	–	–	3.84	0.97

Table 3. Provides elemental compositions for Points 6 and 7 from Fig. 5.

Element	Z	X-ray series	Point 6		Point 7	
			wt.%	at.%	wt.%	at.%
C	6	K	–	–	13.15	37.76
O	8	K	–	–	6.60	14.24
Mg	12	K	–	–	1.13	1.61
Al	13	K	5.18	17.29	0.46	0.62
Si	14	K	–	–	0.39	0.48
Cr	24	K	0.93	1.60	0.57	0.38
Fe	26	K	1.97	3.17	62.15	38.39
Ni	28	K	0.31	0.47	2.53	1.49
Cu	29	K	–	–	3.72	2.02
Pd	46	L	81.61	77.46	9.27	3.01

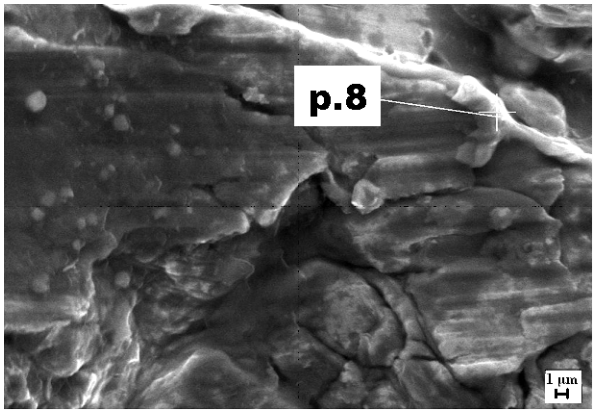

(a)

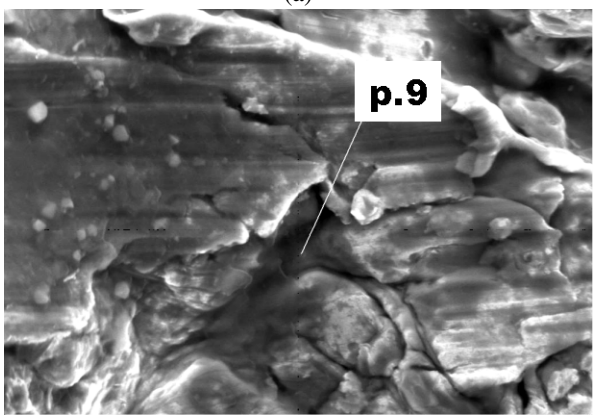

(b)

Figure 6. SEM images of a surface patch near the tapering part from Fig. 2(b).

Table 4. Provides elemental compositions for Points 8 and 9 marked in Fig. 6.

Element	Z	X-ray series	Point 8		Point 9	
			wt.%	at.%	wt.%	at.%
C	6	K	6.42	37.25	17.17	43.80
O	8	K	–	–	14.38	27.54
F	9	K	–	–	3.37	5.44
Na	11	K	–	–	0.82	1.03
Al	13	K	0.42	1.08	0.69	0.79
Si	14	K	–	–	0.40	0.44
P	15	K	–	–	0.26	0.26
Ca	20	K	–	–	0.93	0.71
Cr	24	K	0.39	0.52	–	–
Mn	25	K	–	–	0.18	0.10
Fe	26	K	0.66	0.82	0.33	0.18
Pd	46	L	92.11	60.32	59.52	17.14

As shown here, along with the relatively high palladium concentration, significant amounts of carbon are observed, as in the previously measured surface patch ($_6$C-37.25 at.%). Similarly to the congealed blowouts (see Fig. 2 (a,b)), there is an even greater variety of light atoms of chemical elements such as $_6$C (43.80 at%), $_7$N ↑(?), $_8$O, $_9$F, $_{10}$Ne ↑(?), $_{11}$Na, $_{12}$Mg, $_{13}$Al, $_{14}$Si, $_{15}$P, $_{16}$S, $_{17}$Cl, $_{18}$Ar↑(?), $_{19}$K, $_{20}$Ca, $_{25}$Mn, $_{26}$Fe, and $_{46}$Pd. One can see that all chemical elements are present here, beginning with $Z = 6$ ($_6$C), $Z = 20$ ($_{20}$Ca), where symbols ↑(?) indicate volatile elements which are impossible to register in a non-bound state by microelement analysis.

Figure 7 shows SEM images of two surface patches, also near the tapering part (Fig. 2(b)), with several particles on the palladium surface analyzed using XMA.

It should be noted that all foreign particles in both images are of approximately similar composition, containing significant amounts of rhenium up to 6.03 at.%. Moreover, since these particles are sufficiently small, being up to 1–2 μm in size, the XMA analysis naturally covers also the area around and under these particles. This might account for the "increase" in the palladium concentration, bearing in mind that these particles are most likely comprised of low-melt-point rhenium oxide (Re_2O_7) with the melting temperature around 200°C, which is confirmed by our observation of a very significant concentration of oxygen $_8$O(64.08 at.%) apart from rhenium. It is known that rhenium oxide Re_2O_7 is formed at the temperatures over 150°C in presence of large amounts of oxygen. The boiling temperature for rhenium is slightly above 350°C.

Table 6 shows the elemental compositions for a monocrystal at Points 11 and 12. It is clear that due to the small size of the analyzed crystal, approximately 1.5–2 μm, and its relatively small thickness, the element analysis covers a larger volume than the crystal volume. But even taking account of this, the atomic concentration of rhenium reaches 6.61 at.%. Of special interest is the analysis of the elemental composition in the cracks formed in the palladium wire. It is precisely the areas with noticeable structural disturbances that suffered the most overheating and attendant mechanical stress.

Table 5. Provides the elemental composition for Point 10 indicated in Fig. 7.

Element	*Z*	X-ray series	wt.%	at.%
O	8	K	21.52	64.08
Na	11	K	1.04	2.15
K	19	K	4.22	5.14
Fe	26	K	0.90	0.77
Pd	46	L	48.75	21.83
Re	75	L	23.58	6.03

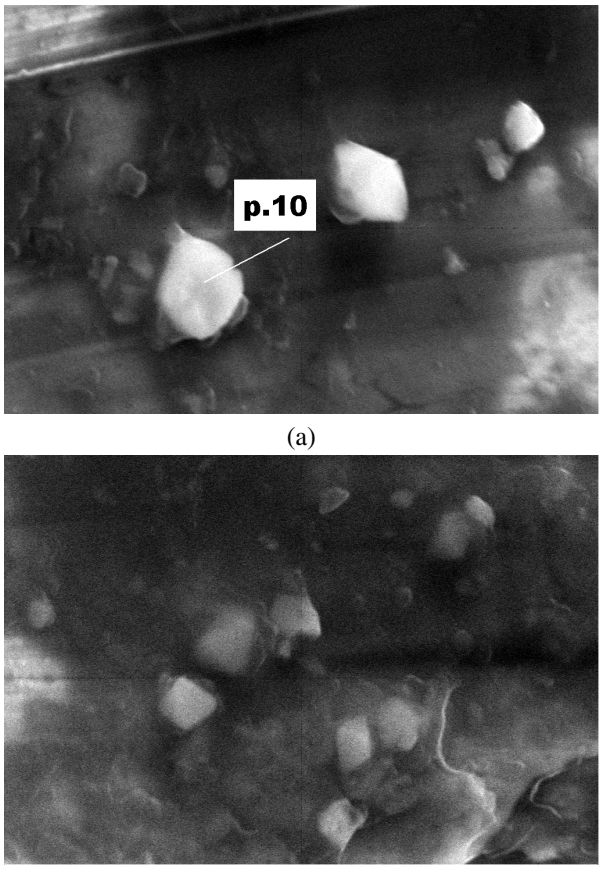

(a)

(b)

Figure 7. SEM images of two surface patches near the tapering part in Fig. 2(b) with foreign particles.

Consequently, this is where nuclear fission reactions with high energy release took place.

It is evident that the element analysis of the crack walls and bottom is not sufficiently reliable (Point 12) but it was not our goal to determine the element concentration with high accuracy. Also, one can observe in the crack significant amounts of silicon ($_{14}$Si–26.89 at.%) in combination with oxygen ($_{8}$O–51.11 at.%).

2.2. Experimental results for a rhenium wire of length 12 mm

It should be noted first and foremost that it was possible to carry out SEM and XMA studies only by using a rhenium wire 12.5 mm long because it had been placed at a distance of 110 mm (behind the palladium wire) from the back wall of the DHPC entrance window. And because it was smaller in size and, consequently, it had acquired a lower induced activity. The other rhenium specimens (of the length 25 and 33 mm) are not accessible for study at the moment due to their high activation level and slow decline of induced activity. Figures 9(a) and (b) provides SEM images of a rhenium wire with the place of entry of γ-quanta (a) and its reverse side (b), respectively.

Figure 10(a) shows a SEM image of surface patch of a rhenium wire 12 mm long near the crack. Once again it is of

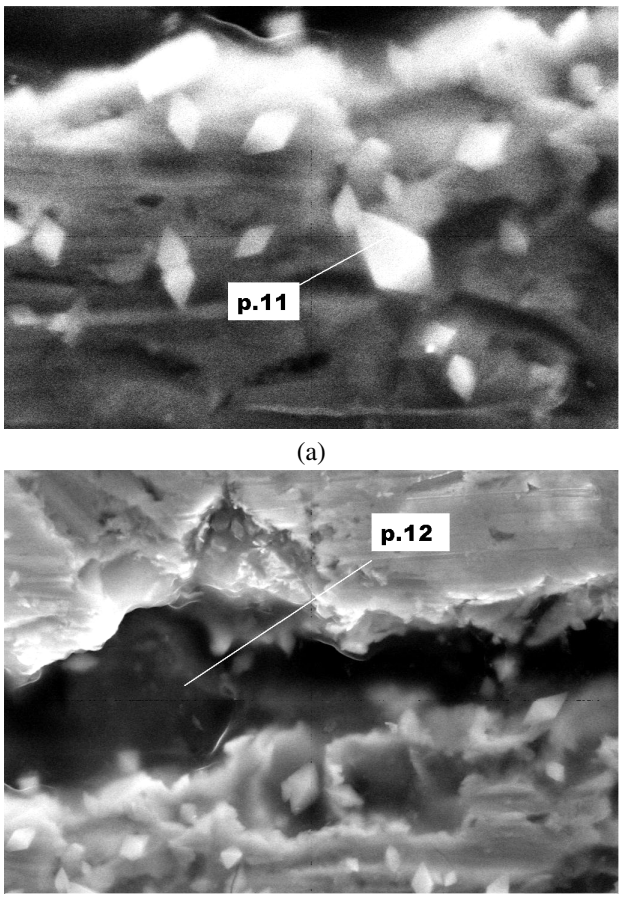

(a)

(b)

Figure 8. SEM images of the crack and hexagonal microcrystals on the side surface of the palladium wire.

interest to estimate the concentrations of impurities produced in nuclear reactions from the most degraded cavities, i.e. from the cracks one of which is presented in Fig. 10 (b). Averaged XMA analysis was carried out over three surface patches. Results are summarized in Table 7.

As one can see, the entire rhenium surface is coated with a carbon layer, with the carbon concentration reaching 80.94 at.%, a rhenium concentration of only 4.92 at.% and relatively high concentration of osmium up to 0.84 at.%

3. Discussions and Conclusions

The results obtained in this study on the changes in the surface structure, bulk properties and chemical composition of palladium and rhenium specimens under irradiation by γ-quanta of a continuous spectrum with the threshold energy 23 MeV confirm our conclusions from previously obtained data on the synthesis of a novel structure and the production of chemical elements lighter than palladium in the DHPC structures (see [1–5]).

In contrast to previous studies [1,2,4], the material of all the DHPC elements in these studies was replaced with

Table 6. The elemental compositions for a monocrystal at Points 11 and 12.

Element	Z	X-ray series	Point 11		Point 12	
			wt.%	at.%	wt.%	at.%
O	8	K	28.60	72.12	29.59	55.11
Na	11	K	0.54	0.95	–	–
Al	13	K	0.42	0.63	0.62	0.69
Si	14	K	–	–	25.35	26.89
S	16	K	0.19	0.23	1.11	1.03
Cl	17	K	0.12	0.14	1.09	0.91
K	19	K	5.60	5.77	1.65	1.26
Ca	20	K	–	–	2.42	1.80
Mn	25	K	0.76	0.56	1.48	0.80
Fe	26	K	1.09	0.79	4.23	2.26
Ni	28	K	–	–	0.68	0.34
Zn	30	K	–	–	0.74	0.34
Pd	46	L	32.19	12.20	30.05	8.41
Re	75	L	30.50	6.61	–	–
Pt	78	L	–	–	0.99	0.15

stainless steel (see Fig. 1) to exclude presence in the chamber of such chemical elements as copper and zinc. The energy of γ-quanta was increased up to 23 MeV to introduce into consideration (γ,n) processes in the giant dipole resonance energy interval [3,5].

Apart from the cracks, significant destruction of the palladium surface and the unusual changed form of the palladium wire end at the spots of entry and exit of γ-quanta (see Fig 2), there were also observed blowouts which resemble congealed "Solar protuberances" and are composed of lighter chemical elements than palladium: $_6$C, $_7$N↑(?), $_8$O, $_9$F, $_{10}$Ne ↑(?), $_{11}$Na, $_{12}$Mg, $_{13}$Al, $_{14}$Si, $_{15}$P, $_{16}$S, $_{17}$Cl, $_{18}$Ar↑(?), $_{19}$K, $_{20}$Ca, $_{22}$Ti, $_{24}$Cr, $_{25}$Mn, $_{26}$Fe, and $_{28}$Ni. Observation of such "protuberances" attests to the presence on the DHPC inner walls from stainless steel (see Fig. 1) of congealed alloy drops composed from the "protuberances" material and to the presence of a synthesized structure on the back wall in the direction of γ-quanta flux, similarly to [1–5]. The "protuberances" allow us to both confirm and explain the formation of the synthesized structure in the special collector from the first experiments described in [1–5].

On the palladium surface one can observe rhenium particles of small size in considerable concentrations (see Figs. 7 and 8, Tables 1, 5 and 6).

As is well known, the melting and sublimation temperatures for rhenium are 3453 and 5873 K [6]. Rhenium has a hexagonal densely packed structure. Oxidation of rhenium occurs at 600°C while in presence of oxygen the metal burns out when heated at the temperature over 400°C. Rhenium oxidation with formation of oxides (ReO_3, Re_2O_7) is observed starting with 300°C, proceeding intensively at the temperatures over 600°C. Rhenium does not interact with hydrogen up to the melting temperature and only absorbs it. However, rhenium can adsorb nine atoms of hydrogen or deuterium, forming $[ReH_9]^{2-}$ or $[ReD_9]^{2-}$ compounds [6,7]. *It is precisely this fact that motivated the authors to test rhenium along with palladium, as well as for the purpose of producing rhenium deuteride.*

Table 7. Results of averaged XMA analysis.

Element	$_6$C	$_8$O	$_{12}$Mg	$_{16}$S	$_{19}$K	$_{20}$Ca	$_{26}$Fe	$_{75}$Re	$_{76}$Os
Initial	–	–		–	–	–	–	100	–
Spectrum 1	65.65	17.44		–	–	–	–	16.07	0.84
Spectrum 2	80.94	13.35		0.25	0.10	–	0.16	4.92	0.28
Spectrum 3	72.95	14.37		–	–	–	–	11.91	0.77
Spectrum 4	72.22	18.90	0.87	0.39	–	1.15	–	6.48	–

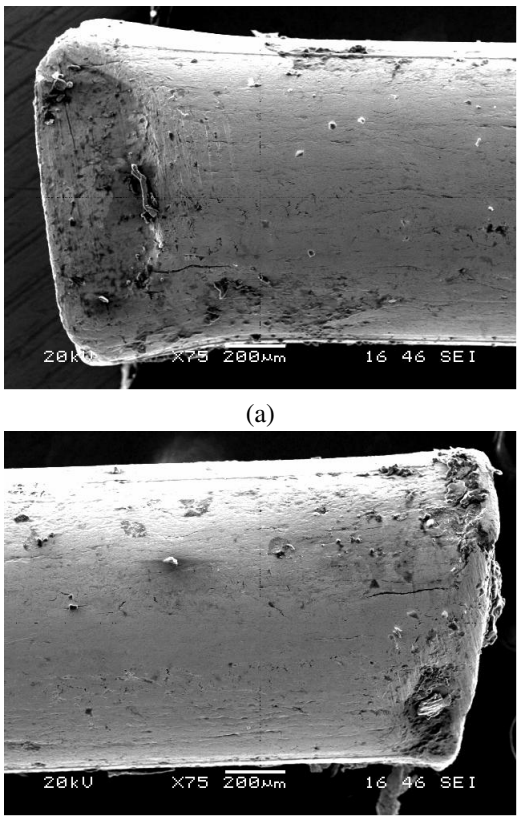

Figure 9. Two sides of a rhenium wire: (a) place of entry of γ-quanta and (b) reverse side.

Rhenium, as contrasted with other high-melting-point metals, does not form carbides. Let us consider specifically the rhenium oxide (VII) Re_2O_7. Its melting and boiling temperatures are $t_{\rm melt}$ = 301°C and t_{boil}=362.4°C [6,7]. Rhenium oxide Re_2O_7 is very volatile at relatively low temperatures; therefore, it evaporates very rapidly from the surface and does not protect rhenium from further oxidation, unlike most of rare-earth metal oxides [6,7]. It sublimates at temperatures above 220°C. Consequently, the rhenium-containing crystallites observed on the surface of palladium are apparently composed of rhenium oxide, which became crystallized near the cracks on cooling (see Figs. 8 and 9).

One can see that there are high concentrations of carbon (see Table 1 – 76.22 and 66.42 at.%, Table 2 – 47.58 at.%, Table 4 – 37.76, 37.25 and 42.80 at.%) and oxygen (Table 5 – 64.08 at.%, Table 6 – 72.12 and 55.11 at.%) in the palladium specimen. The rhenium specimens are marked by high concentrations of carbon (see Table 7 – 65.65, 80.94, 72.95 and 72.22 at.%). In these cases the high carbon concentration is generally accompanied by a significant concentration of oxygen. Conversely, a high oxygen concentration is usually accompanied by considerable carbon concentration. All basic reactions producing lighter elements than palladium are considered in works [3,5]. As was shown in [13,14], the formation of carbon and oxygen in large quantities in nuclear reactions with oxidation of rhenium and other elements is accompanied by the production of relatively heavy elements, which are however lighter than palladium and rhenium, such as $_{38}$Sr, $_{40}$Zr, $_{42}$Mo, and the radioactive elements $_{39}$Y, $_{41}$Nb and $_{70}$Yb, $_{71}$Lu, $_{72}$Hf in the

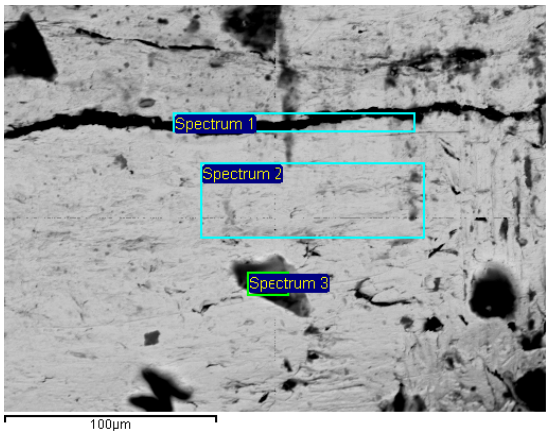

(a)

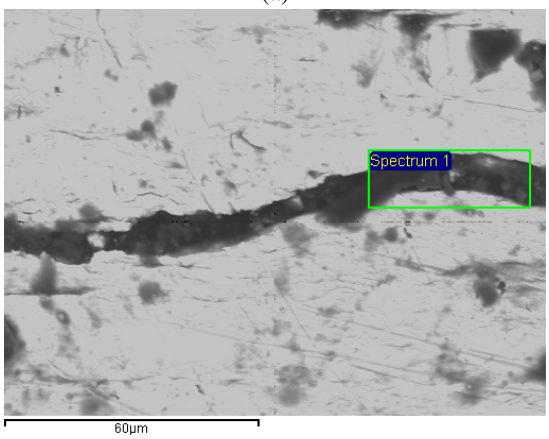

(b)

Figure 10. The surface structure of a rhenium wire with marked patches for XMA analysis.

$_{75}$Re specimen. In this case decay chains up to stable and long-lived decay products are registered. This provides exactly the grounds needed for a detailed presentation of possible Pd and Re fission reactions with decay chains.

It should be noted separately that under the irradiation of the DHPC with rhenium and palladium wires by γ-quanta of energies up to 23 MeV high temperatures with energy release were obtained. This opens up the possibility of constructing deuterated fission reactors (DFR) for power generation, based on deuterium-saturated metals under γ-quanta irradiation [8].

Appendix A.

Consider the Oppenheimer reactions with deuterium [9] in Pd wire (see also [10–12]).

$$\mathrm{d} + {}^{102}_{46}\mathrm{Pd} \rightarrow \mathrm{p} + {}^{103}_{46}\mathrm{Pd}\ [Q = +5.3998\ \mathrm{MeV}] \rightarrow \begin{cases} \xrightarrow{\text{e.c.}} {}^{103}_{45}\mathrm{Rh}\ \ (\text{Stable, } 100\%); \\ \rightarrow {}^{12}\mathrm{C}_6 + {}^{91}_{40}\mathrm{Zr}\ [Q = +0.4145\ \mathrm{MeV}]\ (\text{Stable, } 11.22\%); \end{cases}$$

$$\mathrm{d} + {}^{104}_{46}\mathrm{Pd} \rightarrow \mathrm{p} + {}^{105}_{46}\mathrm{Pd}\ [Q = +4.8688\ \mathrm{MeV}]\ (\text{Stable, } 22.33\%);$$

$$\mathrm{d} + {}^{105}_{46}\mathrm{Pd} \rightarrow \mathrm{p} + {}^{106}_{46}\mathrm{Pd}\ [Q = +7.3378\ \mathrm{MeV}]\ (\text{Stable, } 27.33\%);$$

$$\mathrm{d} + {}^{106}_{46}\mathrm{Pd} \rightarrow \mathrm{p} + {}^{107}_{46}\mathrm{Pd}\ [Q = +4.3048\ \mathrm{MeV}](6.5 \times 10^6\ \text{years}) \xrightarrow{\beta^-} {}^{107}_{47}\mathrm{Ag}\ (\text{Stable, } 51.839\%);$$

$$\mathrm{d} + {}^{108}_{46}\mathrm{Pd} \rightarrow \mathrm{p} + {}^{109}_{46}\mathrm{Pd}\ [Q = +3.9298\ \mathrm{MeV}] \xrightarrow{\beta^-} {}^{109}_{47}\mathrm{Ag}\ \ (\text{Stable, } 48.161\%);$$

$$\mathrm{d} + {}^{110}_{46}\mathrm{Pd} \rightarrow \mathrm{p} + {}^{111}_{46}\mathrm{Pd}\ [Q = +3.5418\ \mathrm{MeV}] \xrightarrow{\beta^-,\beta^-} {}^{111}_{48}\mathrm{Cd}\ \ (\text{Stable, } 12.80\%).$$

As one can see, carbon can be formed only in reactions with $^{102}_{46}$Pd, but the concentration of this isotope is only 1.02%. Correspondingly, in the Oppenheimer reaction it is difficult to obtain the concentrations of oxygen and carbon experimentally detected, since the nuclei forming in this case are stable.

We consider therefore the reactions of the subbarrier fusion of deuterium with the formation and fission of a compound nucleus to the scheme proposed in [10–12].

$$\mathrm{d} + {}^{102}_{46}\mathrm{Pd} \rightarrow {}^{104}_{47}\mathrm{Ag}^{\,*} \rightarrow \begin{cases} {}^{12}_{6}\mathrm{C} + {}^{92}_{41}\mathrm{Nb}_{41}\ [Q = +11.659\ \mathrm{MeV}] \xrightarrow{\text{e.c.},3.5\times10^7\ \text{years}} {}^{92}_{40}\mathrm{Zr}\ (\text{Stable, } 17.15\%); \\ {}^{16}_{8}\mathrm{O} + {}^{88}_{39}\mathrm{Y}\ [Q = +14.246\ \mathrm{MeV}] \xrightarrow{\text{e.c.}} {}^{88}_{38}\mathrm{Sr}\ (\text{Stable, } 82.58\%); \end{cases}$$

$$\mathrm{d} + {}^{104}_{46}\mathrm{Pd} \rightarrow {}^{106}_{47}\mathrm{Ag}^{\,*} \rightarrow \begin{cases} {}^{12}_{6}\mathrm{C}_6 + {}^{94}_{41}\mathrm{Nb}\ [Q = +10.103\ \mathrm{MeV}] \xrightarrow{\beta^-,2.03\times10^4\ \text{years}} {}^{94}_{42}\mathrm{Mo}\ (\text{Stable, } 9.25\%); \\ {}^{16}_{8}\mathrm{O} + {}^{90}_{39}\mathrm{Y}\ [Q = +14.408\ \mathrm{MeV}] \xrightarrow{\beta^-} {}^{90}_{40}\mathrm{Zr}\ (\text{Stable, } 51.45\%); \end{cases}$$

$$\mathrm{d} + {}^{105}_{46}\mathrm{Pd} \rightarrow {}^{107}_{47}\mathrm{Ag}^{\,*} \rightarrow \begin{cases} {}^{12}_{6}\mathrm{O} + {}^{95}_{41}\mathrm{Nb}\ [Q = +11.500\ \mathrm{MeV}] \xrightarrow{\beta^-,34.97\ \text{days}} {}^{95}_{42}\mathrm{Mo}\ (\text{Stable, } 15.92\%); \\ {}^{16}_{8}\mathrm{O} + {}^{91}_{39}\mathrm{Y}\ [Q = +15.800\ \mathrm{MeV}] \xrightarrow{\beta^-,58.51\ \text{days}} {}^{91}_{40}\mathrm{Zr}(1.4 \times 10^4\ \text{years}); \end{cases}$$

$$\mathrm{d} + {}^{106}_{46}\mathrm{Pd}_{46} \rightarrow {}^{108}_{47}\mathrm{Ag}^{*} \rightarrow \begin{cases} {}^{12}_{6}\mathrm{O} + {}^{96}_{41}\mathrm{Nb}\ [Q = +8.831\ \mathrm{MeV}] \xrightarrow{\beta^-,\,23.35\ \mathrm{h}} {}^{96}_{42}\mathrm{Mo}\ (\mathrm{Stable},\ 16.68\%); \\ {}^{16}_{8}\mathrm{O} + {}^{92}_{39}\mathrm{Y}\ [Q = +12.782\ \mathrm{MeV}] \xrightarrow{\beta^-,\,58.51\ \mathrm{d}} {}^{92}_{40}\mathrm{Zr}\ (\mathrm{Stable},\ 17.15\%); \end{cases}$$

$$\mathrm{d} + {}^{108}_{46}\mathrm{Pd} \rightarrow {}^{110}_{47}\mathrm{Ag}^{*} \rightarrow \begin{cases} {}^{12}_{8}\mathrm{O} + {}^{98}_{41}\mathrm{Nb}\ [Q = +7.143\ \mathrm{MeV}] \xrightarrow{\beta^-} {}^{98}_{42}\mathrm{Mo}\ (\mathrm{Stable},\ 24,\ 13\%), \\ {}^{16}_{8}\mathrm{O} + {}^{94}_{39}\mathrm{Y}\ [Q = +10.732\ \mathrm{MeV}] \xrightarrow{\beta^-} {}^{94}_{40}\mathrm{Zr}\ (\mathrm{Stable},\ 17.38\%); \end{cases}$$

$$\mathrm{d} + {}^{110}_{46}\mathrm{Pd} \rightarrow {}^{112}_{47}\mathrm{Ag}^{*} \rightarrow \begin{cases} {}^{12}_{8}\mathrm{O} + {}^{100}_{41}\mathrm{Nb}\ [Q = +4.761\ \mathrm{MeV}] \xrightarrow{\beta^-} {}^{100}_{42}\mathrm{Mo}\ (\mathrm{Stable},\ 9.63\%), \\ {}^{16}_{8}\mathrm{O} + {}^{96}_{39}\mathrm{Y}\ [Q = +7.968\ \mathrm{MeV}] \xrightarrow{\beta^-} {}^{96}_{40}\mathrm{Zr}\ (> 3.56 \times 10^{17}\ \mathrm{years},\ 2.80\%); \end{cases}$$

Consider the formation of carbon and oxygen upon the fission of an excited rhenium nucleus after subbarrier fusion with deuterium:

$$\mathrm{d} + {}^{185}_{75}\mathrm{Re} \rightarrow {}^{187}_{76}\mathrm{Os}^{*} \rightarrow \begin{cases} {}^{12}_{6}\mathrm{O} + {}^{175}_{70}\mathrm{Yb}\ [Q = +24.025\ \mathrm{MeV}] \xrightarrow{\beta^-,\,4.19\ \mathrm{days}} {}^{175}_{71}\mathrm{Lu}\ (\mathrm{Stable},\ 97.41\%); \\ {}^{16}_{8}\mathrm{O} + {}^{171}_{68}\mathrm{Er}\ [Q = +31.785\ \mathrm{MeV}] \xrightarrow{\beta^-,\beta^-} {}^{171}_{70}\mathrm{Yb}_{70}\ (\mathrm{Stable},\ 3.05\%); \end{cases}$$

$$\mathrm{d} + {}^{187}_{75}\mathrm{Re} \rightarrow {}^{189}_{76}\mathrm{Os}^{*} \rightarrow \begin{cases} {}^{12}_{6}\mathrm{O} + {}^{177}_{70}\mathrm{Yb}\ [Q = +22.917\ \mathrm{MeV}] \xrightarrow{\beta^-,\beta^-} {}^{177}_{72}\mathrm{Hf}\ (\mathrm{Stable},\ 18.606\%); \\ {}^{16}_{8}\mathrm{O} + {}^{173}_{68}\mathrm{Er}\ [Q = +30.398\ \mathrm{MeV}] \xrightarrow{\beta^-,\beta^-} {}^{173}_{70}\mathrm{Yb}\ (\mathrm{Stable},\ 16.12\%).. \end{cases}$$

Now, let us consider reactions of the osmium ($_{76}$Os) and tungsten ($_{74}$W) formations:

$$\gamma + {}^{185}_{75}\mathrm{Re} \rightarrow \mathrm{n} + {}^{184}_{75}\mathrm{Re}\ [Q = -7.366\ \mathrm{MeV}] \xrightarrow{\mathrm{e.c.}} \rightarrow {}^{184}_{74}\mathrm{W}(> 3 \times 10^{17}\ \mathrm{years},\ 30.67\%);$$

$$\gamma + {}^{187}_{75}\mathrm{Re} \rightarrow \mathrm{n} + {}^{186}_{75}\mathrm{Re}\ [Q = -7.366\ \mathrm{MeV}] \rightarrow \begin{cases} \xrightarrow{\beta^-} {}^{186}_{76}\mathrm{Os}\ (2 \times 10^{15}\ \mathrm{years},\ 1.58\%); \\ \xrightarrow{\mathrm{e.c.}} {}^{186}_{74}\mathrm{W}\ (\mathrm{Stable},\ 28.6\%). \end{cases}$$

$$\mathrm{n} + {}^{185}_{75}\mathrm{Re} \rightarrow \gamma + {}^{186}_{75}\mathrm{Re}_{75}\ [Q = +6.179\ \mathrm{MeV}] \rightarrow \begin{cases} \xrightarrow{\beta^-} {}^{186}_{76}\mathrm{Os}\ (2 \times 10^{15}\ \mathrm{yaers},\ 1.58\%); \\ \xrightarrow{\mathrm{e.c.}} {}^{186}_{74}\mathrm{W}\ (\mathrm{Stable},\ 28.6\%). \end{cases}$$

$$\mathrm{n} + {}^{187}_{75}\mathrm{Re} \rightarrow \gamma + {}^{188}_{75}\mathrm{Re}\,[Q = +5.872.\ \mathrm{MeV}] \xrightarrow{\beta^-} {}^{188}_{76}\mathrm{Os}_{76}\ (\mathrm{Stable},\ 13.3\%);$$

$$\mathrm{p} + {}^{185}_{75}\mathrm{Re} \rightarrow \gamma + {}^{186}_{76}\mathrm{Os}\,[Q = +6.474.\ \mathrm{MeV}](2 \times 10^{15}\ \mathrm{years},\ 1.58\%);$$

$$\mathrm{p} + {}^{187}_{75}\mathrm{Re}_{75} \rightarrow \gamma + {}^{188}_{76}\mathrm{Os}_{76}\,[Q = +7.209\ \mathrm{MeV}]\ (\mathrm{Stable},\ 13.3\%);$$

$$\mathrm{d} + {}^{185}_{75}\mathrm{Re} \rightarrow \gamma + {}^{187}_{76}\mathrm{Os}\,[Q = 10.542\ \mathrm{MeV}]\ (\mathrm{Stable},\ 1.6\%);\ ;$$

$$\mathrm{d} + {}^{187}_{75}\mathrm{Re} \rightarrow \gamma + {}^{189}_{76}\mathrm{Os}\,[Q = 10.909\ \mathrm{MeV}]\ (\mathrm{Stable},\ 16.1\%)$$

$$\mathrm{d} + {}^{185}_{75}\mathrm{Re} \rightarrow \mathrm{p} + {}^{186}_{75}\mathrm{Re}\,[Q = +3.955\ \mathrm{MeV}] \rightarrow \begin{cases} \xrightarrow{\beta^-} {}^{186}_{76}\mathrm{Os}\ (2 \times 10^{15}\ \mathrm{yaers},\ 1.58\%); \\ \xrightarrow{\mathrm{e.c.}} {}^{186}_{74}\mathrm{W}\ (\mathrm{Stable},\ 28.6\%). \end{cases}$$

$$\mathrm{d} + {}^{187}_{75}\mathrm{Re} \rightarrow \mathrm{p} + {}^{188}_{75}\mathrm{Re}\,[Q = +3.648\ \mathrm{MeV}] \rightarrow {}^{188}_{76}\mathrm{Os}\ (\mathrm{Stable},\ 13.3\%).$$

One can conclude that the formation of a large amount of carbon and oxygen upon the oxidation of rhenium (and other elements as the products of nuclear reactions) must be accompanied by the formation of a sequence of relatively heavy (but lighter than Pd and Re) atoms, such as $_{38}$Sr, $_{40}$Zr, $_{70}$Yb, $_{71}$Lu, and $_{72}$Hf radioactive and stable nuclei. In addition, the disintegration chains up to stable or long-living products should also be registered. This motivates a detailed discussion of possible fission reactions in Pd, Re and the corresponding disintegration chains [13,14].

References

[1] A.Yu. Didyk and R. Wisniewski, Nuclear reactions induced by g–quanta in palladium saturated with deuterium, surrounded by dense deuterium gas, *Eur. Phys. Lett.* **99** (2012) 22001-P1–22001-P6.

[2] A.Yu. Didyk and R. Wisniewski, Chemical composition and structural phase changes of Pd sample and properties of novel synthesized structure at dense deuterium gas under irradiation by γ-quanta, *Phys. Particles and Nucl. Lett.* **9**(8) (2012) 615–631; Preprint E15-2012-34. Dubna. JINR, 2012. 26 p.

[3] A.Yu. Didyk and R. Wisniewski, Phenomenological nuclear reaction description in deuterium saturated palladium and synthesized structure in dense deuterium gas under irradiation by γ-quanta, *Phys. Particles and Nucl. Lett.* 10(4(181)) (2013) 603–611; Preprint E15-2012-35. Dubna. JINR, 2012. 25 p.

[4] A.Yu. Didyk and R. Wisniewski, Synthesis of new structures in dense gaseous deuterium and saturated with deuterium palladium in nuclear reactions induced by γ-quanta, *Phys. Chemi. Materials Processing* **5**(5) (2012) 5–13; Preprint R15-2012-50, Dubna, JINR, 17 p.

[5] A.Yu. Didyk and R. Wisniewski, Nuclear reactions in saturated with deuterium palladium and rhenium in dense deuterium gas under irradiation by γ-quanta of continuous spectrum with threshold energy 23 MeV, *Phys. Particles and Nucl. Lett.* **10**(4) (2013) 381–392; Preprint R15-2012-63. Dubna, 2012, 21 p.

[6] A.Yu. Didyk and R. Wisniewski, Properties of Hydrogen and its Isotopes under High Pressure, and Technological Applications, Monograph, Dubna, 2013, 320 p.
[7] Transition metal hydrides, edited by Earl L. Muetterties (Marcel Deccer, New York, 1971), 342 p.
[8] A.Yu. Didyk, R. Wisniewski and T. Wilczynska-Kitowska, Device for energy production. Patent on Application Model, No. 122198, 21 May 2012.
[9] J.R. Oppenheimer and M. Fillips, Note for the transmission functions for deuteron, *Phys. Rev.* **48**(15) (1935) 500–502.
[10] J.G. Moretto, *Nucl. Phys.* A **247** (1975) 211.
[11] A.J. Sierk, Mass-assymmetric fission of light nuclei, *Phys. Rev.* **55**(6) (1985) 582–583.
[12] A.J. Sierk, Macroscopic model of rotating nuclei, *Phys. Rev.* **55**(6) (1986) 2039–2052.
[13] A.Yu. Didyk and R. Wisniewski, Nuclear reactions in deuterided palladium and rhenium irradiated with a continuous spectrum at a threshold energy of 23 MeV in dense deuterium gas, *Phys. Particles and Nucl. Lett*. **10**(4) (2013) 381–392.
[14] A.Yu. Didyk and R. Wisniewski, The study of changes in the elemental composition changes of Re and Pd samples, irradiated in dense deuterium by γ-quanta of threshold energy 23 MeV, *J. Phys. Sci. Appl.* **3**(4) (2013) 209–217.